QUANTUM INFORMATION

On-demand entanglement of molecules in a reconfigurable optical tweezer array

Connor M. Holland[1]†, Yukai Lu[1,2]†, Lawrence W. Cheuk[1]*

Entanglement is crucial to many quantum applications, including quantum information processing, quantum simulation, and quantum-enhanced sensing. Because of their rich internal structure and interactions, molecules have been proposed as a promising platform for quantum science. Deterministic entanglement of individually controlled molecules has nevertheless been a long-standing experimental challenge. We demonstrate on-demand entanglement of individually prepared molecules. Using the electric dipolar interaction between pairs of molecules prepared by using a reconfigurable optical tweezer array, we deterministically created Bell pairs of molecules. Our results demonstrate the key building blocks needed for quantum applications and may advance quantum-enhanced fundamental physics tests that use trapped molecules.

Entanglement lies at the heart of quantum mechanics. It is central to the practical advantage provided by quantum devices (*1*–*3*) and relevant to understanding the behavior of many-body quantum systems (*4*). The ability to create entanglement controllably has been a long-standing experimental challenge. Molecules have been proposed as a promising platform for quantum simulation and quantum information processing because of their rich internal structure and long-lived interacting states (*5*–*8*). In the past two decades, much progress has been made in producing and controlling molecules at ultracold temperatures, both through coherent assembly of ultracold alkali atoms (*9*) and direct laser-cooling (*10*). Rapid advances have been made in recent years, including the creation of degenerate molecular gases (*11*, *12*), the creation of molecular magneto-optical traps (*10*, *13*–*15*), high-fidelity detection of single molecules (*16*–*18*), and laser-cooling of complex polyatomic molecules (*19*, *20*). In addition, coherent dipolar interactions have been observed in bialkali molecules trapped in optical lattices (*18*, *21*).

A major outstanding challenge to fully realizing the potential of molecules has been achieving deterministic entanglement with microscopic control. In this work, we realized on-demand entanglement between individual laser-cooled molecules trapped in a reconfigurable optical tweezer array (Fig. 1A). The approach of molecular tweezer arrays (*16*, *17*, *22*, *23*) combines the microscopic controllability offered by reconfigurable optical tweezer traps (*24*–*28*) with the ability to generate entanglement through the electric dipolar interaction between molecules. We specifically made use of effective spin-exchange interactions that arise between rotational states to entangle pairs of molecules into Bell states (Fig. 1B) (*29*), which are prototypical maximally entangled states of two particles. Our entanglement protocol implements an iSWAP gate (*8*) that, along with site-resolved single-qubit rotations achievable in our platform through the optical addressing of individual molecules, fulfills the requirement for universal quantum computation.

[1]Department of Physics, Princeton University, Princeton, NJ 08544, USA. [2]Department of Electrical and Computer Engineering, Princeton University, Princeton, NJ 08544, USA.
*Corresponding author. Email: lcheuk@princeton.edu
†These authors contributed equally to this work.

Preparing and initializing arrays of laser-cooled molecules

Our work starts with single laser-cooled calcium monofluoride (CaF) molecules trapped in a dynamically reconfigurable array of optical tweezer traps (*17*, *23*). Through a series of steps involving laser-cooling, optical trapping, and transport, single molecules are transferred from a magneto-optical trap into a one-dimensional (1D) array of 37 identical optical tweezer traps with a uniform spacing of 4.20(6) μm (numbers in parentheses are the standard deviation). Because our laser-cooling scheme relies on a closed optical cycle present only for the $X^2\Sigma(v = 0, N = 1)$ manifold in CaF (*30*)—where v and N denote the molecular vibrational and rotational state, respectively—the molecules loaded into the tweezers occupy a single rovibrational manifold.

To remove the randomness in tweezer occupation, we used a rearrangement approach pioneered in neutral atom experiments (*24*, *25*). We nondestructively detected the tweezer occupations using a variant of Λ-imaging (*31*). The empty tweezers were identified then switched off, and the remaining occupied tweezers were then rearranged into the desired 1D pattern. We characterized the rearrangement procedure by measuring the probability of successfully creating uniform arrays and found a single-particle rearrangement fidelity of 97.4(1)%. As shown in Fig. 2A, we were able to create uniform arrays up to a size of 16, with a probability >0.6. The rearrangement fidelity was limited by the nondestructive detection fidelity, with minimal loss [0.2(10)%] caused by movement of the tweezer traps.

After rearrangement, we initialized the internal state of the molecules, which were distributed among the 12 hyperfine states in the $X^2\Sigma(v = 0, N = 1)$ rovibrational manifold. To prepare molecules into a single hyperfine state, we optically pumped molecules into $|D\rangle = X^2\Sigma(v = 0, N = 1, J = 3/2, F = 2, m_F = 2)$, where J denotes the total angular momentum excluding nuclear spin, F denotes the total angular momentum, and m_F denotes its projection onto the quantization axis. Subsequent microwave sweeps along with an optical clean-out pulse transferred the molecules into the target final state $|\uparrow\rangle = X^2\Sigma(v = 0, N = 1, J = 1/2, F = 0, m_F = 0)$ (Fig. 2C). The overall fidelity of preparing molecules in $|\uparrow\rangle$ was 82.4(11)%. Our preparation sequence ensures that the dominant preparation error is in the form of unoccupied tweezers, with a small contribution coming from molecules prepared in the incorrect internal state $|+\rangle = X^2\Sigma(v = 0, N = 0, J = 1/2, F = 1, m_F = 1)$. The state initialization errors come from imperfect microwave transfer, polarization impurity of the optical pumping light, and loss caused by heating in the tweezer traps. After state preparation, we measured a molecular temperature of T = 151(10) μK.

Probing rotational coherence of single molecules

To produce entanglement through the dipolar interactions between molecules, we required long coherence times compared with the typical interaction timescales of ~10 ms at our tweezer separations. Achieving long coherence times for optically trapped molecules has been an ongoing experimental challenge, with steady advances being made. For molecules, different internal states can experience different trapping potentials that, in combination with motion caused by finite temperature, can lead to decoherence. For $^1\Sigma$ bialkali molecules, long coherence times of different nuclear spin states have been reported (*32*). Work using "magic" trapping conditions has also demonstrated extended coherence times between rotational states in both $^1\Sigma$ and $^2\Sigma$ molecules (*18*, *33*–*36*).

Because the effective spin-exchange interactions couple different rotational states, we wanted long rotational coherence times between the two interacting states $|\uparrow\rangle$ and $|\downarrow\rangle = X^2\Sigma(v = 0, N = 0, J = 1/2, F = 1, m_F = 0)$. Building on previous work in CaF (*36*), we identified a pseudo-magic trapping condition in which both spin states experience approximately identical trapping potentials. Our pseudo-magic condition takes into account vector and tensor shifts and is achieved by applying a magnetic field orthogonal to the tweezer light polarization at a reduced tweezer depth

compared with that used for initial loading and imaging.

To measure the resulting coherence time, we prepared pairs of tweezer traps in which one trap is empty and the other is occupied by a molecule initialized in $|\uparrow\rangle$. We next applied a Ramsey pulse sequence consisting of two $\pi/2$ microwave pulses (first pulse along $\hat{x}$, second pulse along $\hat{n} = \cos\theta\hat{x} + \sin\theta\hat{y}$) separated by a variable free evolution time (Fig. 3A). The remaining fraction of $|\uparrow\rangle$ molecules, $P_\uparrow$, oscillates as a function of θ, with the oscillation amplitude directly measuring the coherence. Fitting to an exponential decay curve yields a bare coherence time T_2^* of 2.5(3) ms. Adding a spin-echo improves the coherence time to T_2 = 29(2) ms. Following previous work that explored dipolar interactions of KRb molecules in an optical lattice (*21*, *37*), we implemented the XY8 dynamical decoupling sequence depicted in Fig. 3B and found that the $1/e$ coherence time was further extended to 215(30) ms (Fig. 3C). This is consistent with our understanding that the bare coherence times are primarily limited by slow (millisecond timescale) fluctuations of ambient magnetic fields.

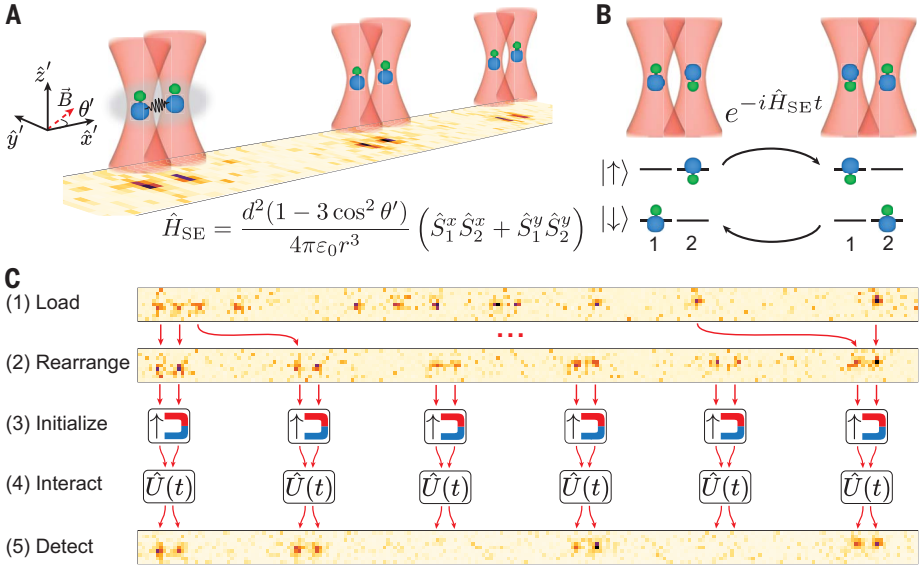

Fig. 1. Laser-cooled molecules in a reconfigurable optical tweezer array. (**A**) Single CaF molecules trapped in an optical tweezer array are prepared into closely separated tweezer pairs. Molecules in each pair held by separate tweezer traps interact through the long-range electric dipolar interaction $\hat{H}_{SE}$. (**B**) The electric dipolar interaction leads to dipolar spin-exchange of rotational excitations. (**C**) Molecules are loaded stochastically, detected nondestructively, and rearranged into the desired 1D configuration. The molecules are then initialized into a single internal state, and the pair separations are reduced to switch on interactions. After specific interaction times, the pairs are separated and detected state-selectively.

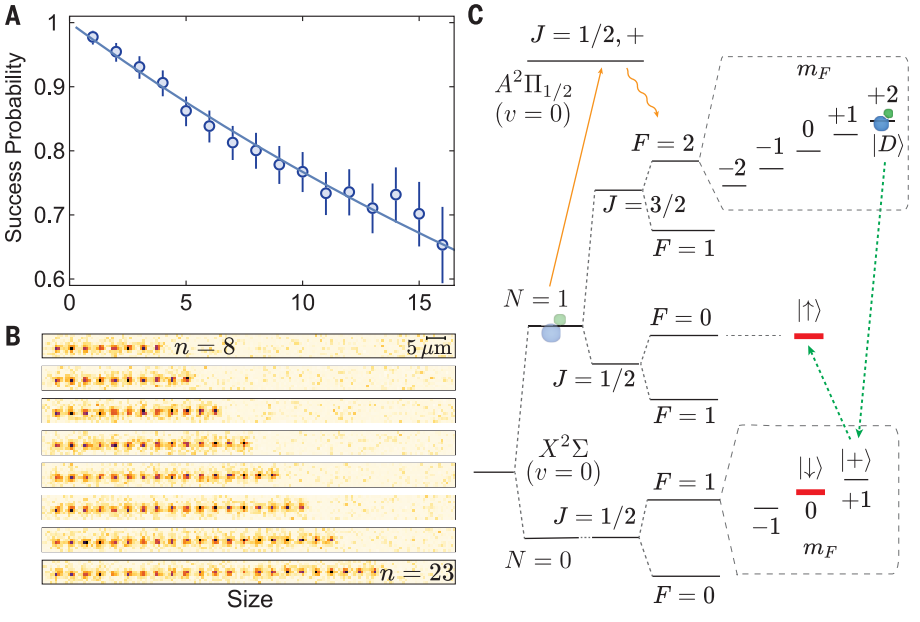

Fig. 2. Tweezer rearrangement and internal state initialization. (**A**) Probability of creating defect-free molecular arrays through rearrangement. A fit to p^n, where n is the array size, gives a single-particle rearrangement fidelity of p = 0.974(1). (**B**) Example images of defect-free arrays. (**C**) Optical pumping (orange arrow) prepares molecules in $|D\rangle$. Microwave sweeps (dashed green arrows) transfer $|D\rangle$ molecules to $|\uparrow\rangle$.

Observing coherent intermolecular interactions

Having achieved sufficiently long rotational coherence times, we next set out to observe coherent spin-exchange interactions. The long-range electric dipolar interaction between the molecules gives rise to resonant exchange of rotational excitations between $|\uparrow\rangle$ and $|\downarrow\rangle$. The resulting spin-exchange interaction is described by the Hamiltonian

$$H_{SE} = \frac{J}{2}\left(\hat{S}_1^+\hat{S}_2^- + \hat{S}_1^-\hat{S}_2^+\right) = J\left(\hat{S}_1^x\hat{S}_2^x + \hat{S}_1^y\hat{S}_2^y\right)$$

where $\hat{S}_i^+, \hat{S}_i^-, \hat{S}_i^x, \hat{S}_i^y$ are spin-1/2 operators for molecule i and

$$J = \frac{d^2}{4\pi\varepsilon_0}\frac{1}{r^3}\left(1 - 3\cos^2\theta'\right)$$

with $d = \langle\uparrow|\hat{\mathbf{d}}|\downarrow\rangle$ being the transition dipole moment, $r = |\vec{r}|$ being the intermolecular separation, θ' being the angle between $\vec{r}$ and the quantization axis, and ε_0 being the free space permittivity. Starting with two molecules in a product state, time evolution under $\hat{H}_{SE}$ can lead to entanglement. For example, two molecules initially prepared in the product state $|\uparrow\rangle \otimes |\downarrow\rangle$ become maximally entangled after interacting for a time $t = \pi\hbar/(2J)$, where $\hbar$ is Planck's constant h divided by 2π. In our system, the quantization axis is orthogonal to the intermolecular separation—that is, θ' = 90°.

To observe the effect of spin-exchange interactions, we first created pairs of $|\uparrow\rangle$ molecules at an initial separation of 4.20(6) μm, over which interactions were negligible. We next reduced the pair separation to 1.93(3) μm over 3 ms, at which the interaction strength J ($J = \hbar \times 43$ Hz) becomes appreciable on the coherence timescale. Subsequently, we applied the Ramsey pulse sequence used above with θ = 0. To retain long coherence times, the XY8 decoupling pulses were kept on during the free

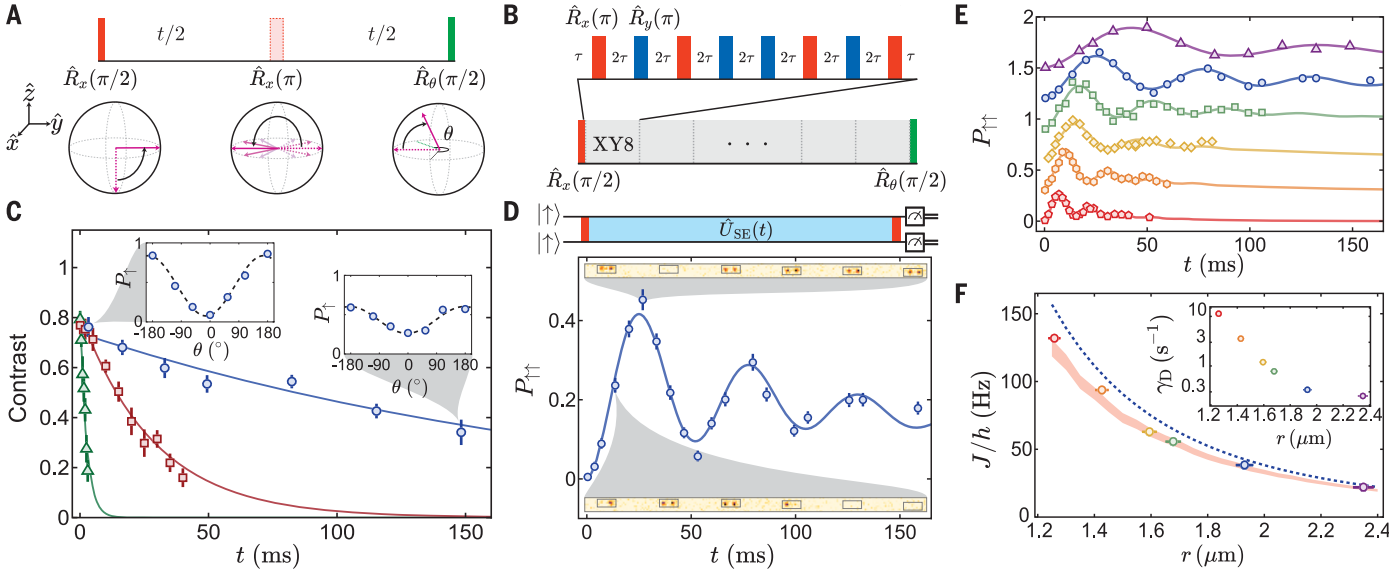

Fig. 3. Single-particle coherence and spin-exchange oscillations. (**A**) Ramsey pulse sequence used to measure rotational coherence. (Bottom) Bloch sphere diagrams show the action of the various pulses for a molecule initialized in $|\downarrow\rangle$. (**B**) The XY8 dynamical decoupling sequence. (**C**) Ramsey contrast of noninteracting molecules versus free evolution time t. Green triangles, red squares, and blue circles indicate the cases for which no spin-echo, one spin-echo, and the XY8 sequence is applied, respectively. Exponential fits give coherence times ($1/e$) of 2.5(3) ms, 29(2) ms, and 215(30) ms, respectively. (Insets) Ramsey fringes with corresponding sinusoidal fits indicated with the dashed lines. (**D**) Spin-exchange oscillations at a tweezer separation of 1.93(3) μm. Shown are the $|\uparrow\uparrow\rangle$ populations measured after the Ramsey pulse sequence, $P_{\uparrow\uparrow}$, as a function of interaction time t, for molecular pairs initialized in $|\uparrow\uparrow\rangle$. The solid curve is a fit to a phenomenological model. (Insets) Fluorescence images at the indicated times. (**E**) Spin-exchange oscillations at separations of 1.26(2) μm (red pentagons), 1.43(2) μm (orange hexagons), 1.60(2) μm (yellow diamonds), 1.68(2) μm (green squares), 1.93(3) μm (blue circles), and 2.35(3) μm (purple triangles). Curves are offset vertically by 0.3 for clarity. (**F**) The extracted spin-exchange strength J versus pair separation r. The light red band indicates the theoretical prediction taking into account the finite temperature of the molecules and the uncertainty in the electric dipole moment of CaF. The dashed blue curve indicates the prediction without taking into account finite temperature. (Inset) The single-particle loss rate γ_D versus pair separation r.

evolution time. Because the π-pulses in the XY8 sequence leave $\hat{H}_{SE}$ unchanged, spin-exchange interactions are preserved (*38*).

For a molecular pair initialized in $|\uparrow\uparrow\rangle$, the resulting state after the Ramsey sequence is given by

$$|\psi\rangle = ie^{-i\frac{Jt}{4\hbar}}\left[\sin\left(\frac{Jt}{4\hbar}\right)|\uparrow\uparrow\rangle + i\cos\left(\frac{Jt}{4\hbar}\right)|\downarrow\downarrow\rangle\right] \quad (1)$$

and $P_{\uparrow\uparrow}$ oscillates at an angular frequency of $J/(2\hbar)$. As shown in Fig. 3D, we observed oscillations of $P_{\uparrow\uparrow}$, directly revealing the presence of coherent spin-exchange interactions. By varying the pair separation between 1.26(2) and 2.35(3) μm, we verified that the interaction strength J, as extracted from the oscillation frequency, approximately scales as $1/r^3$, as expected for dipolar interactions (Fig. 3F). Experiments with bulk samples of bialkali molecules in optical lattices have observed coherent spin-exchange both through macroscopic measurements (*21*, *37*) and with single-molecule resolution (*18*), whereas in this work, we observed coherent interactions between individually prepared, laser-cooled molecules.

Examining the $P_{\uparrow\uparrow}$ oscillations in detail, we found that they damp more quickly when the molecules are closer. This could arise from increased molecular loss and reduced single-particle coherence times at close separations. Additionally, the thermal motion of molecules gives rise to disorder in the spin-exchange coupling constant J through variations in the intermolecular separations, leading to damping. At a fixed molecular temperature, this effect increases at closer separations. To determine which damping mechanism is dominant, we first measured single-particle loss rates and found that they increase at close separations (Fig. 3F, inset). We believe that the loss is caused by parametric heating specific to our scheme of generating tweezer traps using an acousto-optical deflector (AOD) and can be circumvented with other tweezer-generation techniques. Molecular loss, however, does not account for all of the observed damping, especially at close separations. Independently measured single-particle decoherence rates are also insufficient to explain the damping. This leaves finite molecular temperature as the dominant cause of damping at close distances. Simulations that used experimentally measured temperatures revealed damping rates comparable with the observations (supplementary text and fig. S2) (*39*).

Creating and verifying entanglement of molecules

Having established the presence of coherent spin-exchange interactions, we next used them to entangle molecules. Specifically, as proposed in (*8*), time evolution by $\hat{H}_{SE}$ for a specific time of $T = \pi\hbar/J$ implements an iSWAP gate, which is maximally entangling. By applying two additional π/2 pulses along the x axis before and after the iSWAP gate, one can convert a molecular pair prepared in $|\uparrow\uparrow\rangle$ into the Bell state $|\psi_B\rangle = \frac{1}{\sqrt{2}}(|\uparrow\uparrow\rangle + i|\downarrow\downarrow\rangle)$, which is maximally entangled. As a compromise between maximizing J and minimizing heating loss, we chose a pair separation of 1.93(3) μm for creating $|\psi_B\rangle$.

To demonstrate entanglement of molecules, we measured the Bell state creation fidelity $\mathcal{F} = \langle\psi_B|\rho|\psi_B\rangle$, where ρ is the experimentally obtained density matrix. As pointed out in (*40*), $\mathcal{F}$ acts as an entanglement witness, with $\mathcal{F} > 1/2$ indicating two-particle entanglement. To extract $\mathcal{F}$ experimentally, we made use of the relation (*41*)

$$\mathcal{F} = \frac{1}{2}\left(P_{\uparrow\uparrow} + P_{\downarrow\downarrow} + \mathcal{C}\right) \quad (2)$$

where $P_{\uparrow\uparrow}$ and $P_{\downarrow\downarrow}$ are the probabilities of measuring $|\uparrow\uparrow\rangle$ and $|\downarrow\downarrow\rangle$, respectively, and $\mathcal{C}$ is the amplitude of the coherence between $|\uparrow\uparrow\rangle$ and $|\downarrow\downarrow\rangle$.

To measure $P_{\uparrow\uparrow}$, we separated the two molecules after preparing $|\psi_B\rangle$ and subsequently

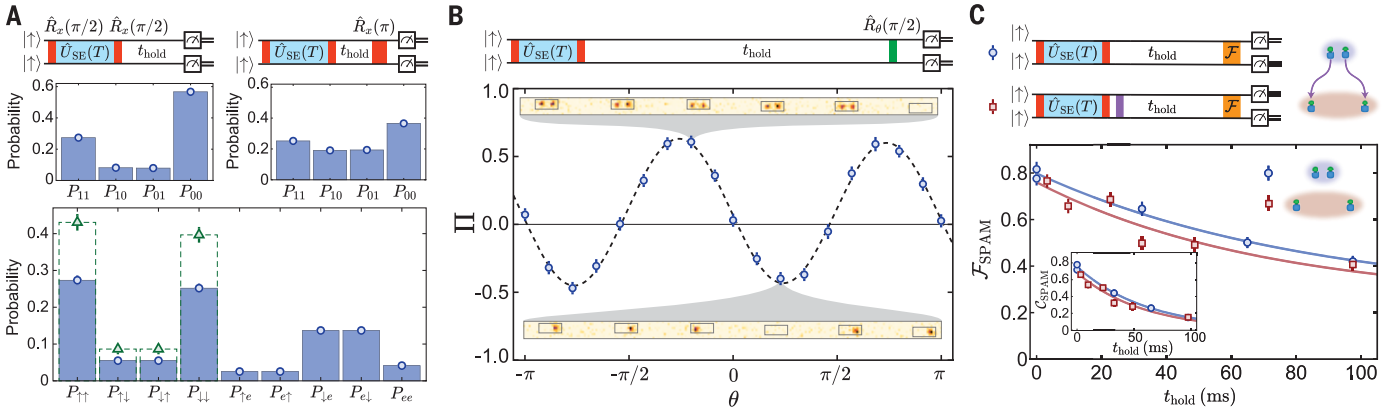

Fig. 4. Creating and probing Bell pairs. (**A**) (Top left) The two-tweezer detection probabilities P_{ij} for the Bell pairs. (Top right) Corresponding probabilities when an additional π pulse is applied before measurement. (Bottom) The full probabilities extracted from top left and top right. The SPAM-corrected populations for the $|\uparrow\rangle - |\downarrow\rangle$ subsystem are indicated with the green triangles. (**B**) Probing Bell state coherence through parity oscillations. The coherence $\mathcal{C}$ between $|\uparrow\uparrow\rangle$ and $|\downarrow\downarrow\rangle$ is obtained from the amplitude of the oscillations in Π as a function of θ. (Insets) Example images at the maxima and minima of Π. (**C**) SPAM-corrected Bell state fidelity $\mathcal{F}_{\mathrm{SPAM}}$ versus hold time t at the initial pair creation distance of 1.93(3) μm are indicated with blue circles. Red squares indicate the corresponding data for pairs separated to a larger distance of 4.20(6) μm after creation. (Inset) The contrast $\mathcal{C}_{\mathrm{SPAM}}$ versus hold time t for the two separations. The extracted 1/e lifetimes are ($\mathcal{F}_{\mathrm{SPAM}}$, $\mathcal{C}_{\mathrm{SPAM}}$) = [85(5) ms, 61(3) ms] at the Bell creation distance, and [70(16) ms, 57(8) ms] at the larger separation.

measured the probability that both tweezers in a pair appear bright. Because our imaging scheme detects only $|\uparrow\rangle$ molecules, to measure $P_{\downarrow\downarrow}$ we applied an additional π-pulse before detection (Fig. 4A) to convert molecules from $|\downarrow\rangle$ to $|\uparrow\rangle$. To obtain the coherence envelope $\mathcal{C}$, we measured parity oscillations as follows. We applied a π/2 pulse about a variable axis $\hat{n} = \cos\theta\hat{x} + \sin\theta\hat{y}$ after preparing $|\psi_B\rangle$. From the two-tweezer probabilities P_{ij}, we constructed the parity signal $\Pi = P_{11} + P_{00} - P_{10} - P_{01}$, where 1 and 0 denote a bright or dark tweezer site, respectively.

For a general density matrix that includes the possibility of empty tweezers ($|e\rangle$) caused by imperfect state preparation, Π can display modulation periodic in 2θ and θ. The 2θ modulation is directly related to the coherence between $|\uparrow\uparrow\rangle$ and $|\downarrow\downarrow\rangle$, whereas the θ modulation is related to single-molecule coherences, such as that between $|e\uparrow\rangle$ and $|e\downarrow\rangle$. The amplitude of the 2θ modulation directly gives $\mathcal{C}$. As shown in Fig. 4B, we found that Π displays modulation periodic in 2θ. The lack of oscillations periodic in θ is consistent with the pulse sequence used. Single molecules prepared in $|e\uparrow\rangle$ or $|\downarrow e\rangle$ effectively experienced a π-pulse, and no single particle coherence was created.

From the population and parity oscillation measurements, we obtained a raw Bell state fidelity of $\mathcal{F}_{\mathrm{RAW}} = 0.524(6)$. Correcting for detection errors, we obtained a Bell state fidelity $\mathcal{F} = 0.540(7)$. The raw and measurement-corrected fidelities were above 1/2, showing that entanglement was indeed present and created on demand.

Correcting additionally for state preparation errors, we obtained a state-preparation and measurement (SPAM)–corrected fidelity of $\mathcal{F}_{\mathrm{SPAM}} = 0.80(2)$. In the context of quantum information processing, the SPAM-corrected Bell state fidelity provides an indication of the quality of the iSWAP gate implemented through spin exchange. Nevertheless, full characterization of our iSWAP gate and a measurement of its fidelity will require full quantum process tomography. With relevance to quantum simulation, our measurements of spin-exchange interactions demonstrate the fundamental building block for simulating XY spin models. In particular, the phase of the 2θ oscillation in parity measures the relative phase between $|\uparrow\uparrow\rangle$ and $|\downarrow\downarrow\rangle$ in the Bell state, which is sensitive to the sign of J. The observed phase of the oscillation shows that $J > 0$, indicating antiferromagnetic spin-exchange interactions. In addition to quantum information processing and quantum simulation, the ability to create entanglement in our system also paves the way toward quantum-enhanced metrology with trapped molecules (*42*).

Having demonstrated deterministic creation of Bell pairs, we next probed their lifetime. We measured the Bell state fidelity $\mathcal{F}_{\mathrm{SPAM}}$ as a function of hold time and found a lifetime of 85(5) ms, which is largely consistent with but somewhat shorter than that expected from uncorrelated single-particle decoherence. We also examined whether the Bell pairs survive when separated to larger distances after their creation. Specifically, we separated the Bell pairs to a distance of 4.20(6) μm over 3 ms after their creation and measured $\mathcal{F}_{\mathrm{SPAM}}$ as a function of hold time. Within experimental uncertainty, we found a lifetime identical to the case without separation (Fig. 4C). This ability to preserve entanglement while separating molecules could allow one to bypass the limited range of dipolar interactions through movement of molecules and obtain arbitrary connectivity useful for quantum simulation and information processing. Similar abilities to preserve entanglement have recently been demonstrated in atomic tweezer arrays (*43*).

Last, we examined how Bell state fidelities can be improved. The measurement-corrected fidelities were affected substantially by state preparation infidelity, which is caused by a variety of technical imperfections such as incomplete microwave transfers. A detailed accounting of errors shows that state preparation fidelities exceeding 0.95 can be achieved (*39*). Separately, the SPAM-corrected Bell state fidelity, which reflects the quality of the iSWAP gate, is substantially affected by the finite molecular temperature. To reveal the importance of state preparation fidelity and molecular temperature, we implemented an alternate state preparation procedure (*39*) that both provides a higher state preparation fidelity [0.85(1)] and a lower molecular temperature [T = 107(5) μK]. The resulting fidelities without state preparation correction were improved to $\mathcal{F}_{\mathrm{RAW}} = 0.608(14)$ and $\mathcal{F} = 0.629(14)$, revealing the importance of state preparation (two-tweezer probabilities and parity oscillation data are provided in fig. S4) (*39*). In addition, $\mathcal{F}_{\mathrm{SPAM}}$ improves to 0.863(25) (*39*), suggesting that molecular temperature is a key factor in achieving high-fidelity entanglement.

Discussion and Outlook

The observed dependence of SPAM-corrected Bell state fidelities on temperature agrees well with numerical simulations, which indicate that lowering the molecular temperatures further by a factor of ~10 could allow fidelities to reach the 0.99 level (*39*). Such further cooling could be achieved with methods such as Raman sideband cooling for molecules

(*44*, *45*). Further improvements are also possible through optimized entanglement schemes. Recent theoretical work that used quantum optimal control has proposed a robust two-qubit entangling gate for CaF molecules in tweezer traps that provides entanglement fidelities exceeding 0.999, under the assumption that they are cooled near their motional ground state (*46*).

We have demonstrated on-demand entanglement of molecules in a reconfigurable optical tweezer array. Our work was enabled by several advances we have made in controlling laser-cooled molecules, including initialization of defect-free molecular arrays, achievement of long rotational coherence times in tightly focused tweezer traps, and observation of coherent dipolar interactions between individual laser-cooled molecules. The ability to entangle molecules on demand is a key building block toward simulating quantum spin models, processing quantum information, and performing quantum-enhanced measurements in the emerging platform of molecular tweezer arrays. Specifically for quantum simulation and information processing, the interactions between long-lived molecular states could offer long evolution times and deep circuit depths. With further advances in lowering molecular temperatures, molecular tweezer arrays could potentially provide performance similar to that of established platforms such as Rydberg atom arrays, trapped ions, and superconducting qubits. Our work on entangling molecules on demand, combined with the recent rapid progress in extending laser-cooling to molecular species of increasing complexity (*19*, *20*), opens research avenues such as quantum-enhanced precision measurement by using trapped molecules (*47*) and explorations of molecular collisions (*48*) and chemical reactions with entangled matter.

After the initial submission of this work, we became aware of related work reporting dipolar spin-exchange and entanglement between molecules in an optical tweezer array (*49*).

REFERENCES AND NOTES

1. M. A. Nielsen, I. L. Chuang, *Quantum Computation and Quantum Information* (Cambridge, Univ. Press, 2010).
2. N. Gisin, G. Ribordy, W. Tittel, H. Zbinden, *Rev. Mod. Phys.* **74**, 145–195 (2002).
3. J. Preskill, *Quantum* **2**, 79 (2018).
4. L. Amico, R. Fazio, A. Osterloh, V. Vedral, *Rev. Mod. Phys.* **80**, 517–576 (2008).
5. D. DeMille, *Phys. Rev. Lett.* **88**, 067901 (2002).
6. L. D. Carr, D. DeMille, R. V. Krems, J. Ye, *New J. Phys.* **11**, 055049 (2009).
7. J. A. Blackmore *et al*., *Quantum Sci. Technol.* **4**, 014010 (2018).
8. K.-K. Ni, T. Rosenband, D. D. Grimes, *Chem. Sci.* **9**, 6830–6838 (2018).
9. K.-K. Ni *et al*., *Science* **322**, 231–235 (2008).
10. J. F. Barry, D. J. McCarron, E. B. Norrgard, M. H. Steinecker, D. DeMille, *Nature* **512**, 286–289 (2014).
11. L. De Marco *et al*., *Science* **363**, 853–856 (2019).
12. A. Schindewolf *et al*., *Nature* **607**, 677–681 (2022).
13. S. Truppe *et al*., *Nat. Phys.* **13**, 1173–1176 (2017).
14. L. Anderegg *et al*., *Phys. Rev. Lett.* **119**, 103201 (2017).
15. A. L. Collopy *et al*., *Phys. Rev. Lett.* **121**, 213201 (2018).
16. L. R. Liu *et al*., *Science* **360**, 900–903 (2018).
17. L. Anderegg *et al*., *Science* **365**, 1156–1158 (2019).
18. L. Christakis *et al*., *Nature* **614**, 64–69 (2023).
19. D. Mitra *et al*., *Science* **369**, 1366–1369 (2020).
20. N. B. Vilas *et al*., *Nature* **606**, 70–74 (2022).
21. B. Yan *et al*., *Nature* **501**, 521–525 (2013).
22. J. T. Zhang *et al*., *Quantum Sci. Technol.* **7**, 035006 (2022).
23. C. M. Holland, Y. Lu, L. W. Cheuk, *Phys. Rev. Lett* **131**, 053202 (2023).
24. M. Endres *et al*., *Science* **354**, 1024–1027 (2016).
25. D. Barredo, S. de Léséleuc, V. Lienhard, T. Lahaye, A. Browaeys, *Science* **354**, 1021–1023 (2016).
26. A. Cooper *et al*., *Phys. Rev. X* **8**, 041055 (2018).
27. M. A. Norcia, A. W. Young, A. M. Kaufman, *Phys. Rev. X* **8**, 041054 (2018).
28. S. Saskin, J. T. Wilson, B. Grinkemeyer, J. D. Thompson, *Phys. Rev. Lett.* **122**, 143002 (2019).
29. J. S. Bell, *Physics Physique Fizika* **1**, 195–200 (1964).
30. B. K. Stuhl, B. C. Sawyer, D. Wang, J. Ye, *Phys. Rev. Lett.* **101**, 243002 (2008).
31. L. W. Cheuk *et al*., *Phys. Rev. Lett.* **121**, 083201 (2018).
32. J. W. Park, Z. Z. Yan, H. Loh, S. A. Will, M. W. Zwierlein, *Science* **357**, 372–375 (2017).
33. B. Neyenhuis *et al*., *Phys. Rev. Lett.* **109**, 230403 (2012).
34. F. Seeßelberg *et al*., *Phys. Rev. Lett.* **121**, 253401 (2018).
35. J. Lin, J. He, X. Ye, D. Wang, *Phys. Rev. A* **103**, 023332 (2021).
36. S. Burchesky *et al*., *Phys. Rev. Lett.* **127**, 123202 (2021).
37. J.-R. Li *et al*., *Nature* **614**, 70–74 (2023).
38. J. Choi *et al*., *Phys. Rev. X* **10**, 031002 (2020).
39. Experimental and simulation methods, additional supporting data, and supplementary text are available as supplementary materials.
40. C. A. Sackett *et al*., *Nature* **404**, 256–259 (2000).
41. Q. A. Turchette *et al*., *Phys. Rev. Lett.* **81**, 3631–3634 (1998).
42. L. Pezzè, A. Smerzi, M. K. Oberthaler, R. Schmied, P. Treutlein, *Rev. Mod. Phys.* **90**, 035005 (2018).
43. D. Bluvstein *et al*., *Nature* **604**, 451–456 (2022).
44. L. Caldwell, M. Tarbutt, *Phys. Rev. Res.* **2**, 013251 (2020).
45. Y. Lu, S. J. Li, C. M. Holland, L. W. Cheuk, Raman sideband cooling of molecules in an optical tweezer array. arXiv:2306.02455v1 [physics.atom-ph] (2023).
46. M. Hughes *et al*., *Phys. Rev. A* **101**, 062308 (2020).
47. B. L. Augenbraun *et al*., *New J. Phys.* **22**, 022003 (2020).
48. L. W. Cheuk *et al*., *Phys. Rev. Lett.* **125**, 043401 (2020).
49. Y. Bao *et al*., Dipolar spin-exchange and entanglement between molecules in an optical tweezer array. arXiv:2211.09780v1 [physics.atom-ph] (2023).
50. L. W. Cheuk, C. M. Holland, Y. Lu, On-demand entanglement of molecules in a reconfigurable optical tweezer array. Dryad (2023); https://doi.org/10.5061/dryad.j9kd51chh.
51. L. W. Cheuk, C. M. Holland, Y. Lu, On-demand entanglement of molecules in a reconfigurable optical tweezer array. Zenodo (2023); https://doi.org/10.5281/zenodo.8140983.

ACKNOWLEDGMENTS

We thank S. J. Li, W. Bakr's group, S. Gopalakrishnan, and J. Thompson for fruitful discussions. We also thank W. Bakr, J. Thompson, S. J. Li, and C. Chiu for careful readings of the manuscript. **Funding:** This work was supported by National Science Foundation grant 2207518, the Alfred P. Sloan Foundation, and Princeton University. **Author contributions:** Conceptualization: L.W.C. Methodology: C.M.H., Y.L., and L.W.C. Investigation: C.M.H., Y.L., and L.W.C. Visualization: C.M.H., Y.L., and L.W.C. Funding acquisition: L.W.C. Supervision: L.W.C. Writing – original draft: C.M.H., Y.L., and L.W.C. Writing – review and editing: C.M.H., Y.L., and L.W.C. **Competing interests:** The authors declare that they have no competing interests. **Data and materials availability:** Data and code are available at Dryad (*50*) and Zenodo (*51*). **License information:** Copyright © 2023 the authors, some rights reserved; exclusive licensee American Association for the Advancement of Science. No claim to original US government works. https://www.science.org/about/science-licenses-journal-article-reuse

SUPPLEMENTARY MATERIALS

science.org/doi/10.1126/science.adf4272
Materials and Methods
Supplementary Text
Figs. S1 to S5
Table S1
References (*52*–*56*)

Submitted 20 October 2022; resubmitted 30 November 2022
Accepted 28 September 2023
10.1126/science.adf4272